4 Sediment Measurements and Experiments

Sediment conditions and characteristics, especially as they pertain to resuspension, transport and deposition, affect possible impacts of dredged material on water-column conditions and must be specified in the numerical sediment model. Grain-size distribution, bulk sediment density, settling velocity, and erosion parameters are some example characteristics of interest. Information on bed sediment grain-size characteristics was available from other studies (White et al. 1986; White et al. 1989; Morton et al. 1997) and was used and supplemented by new information developed by this study. Laboratory experiments were performed to identify the erosion and settling characteristics of natural bay sediments and simulated dredged material.

Settling Experiments

A limited number of field floc settling tests were performed. A more extensive series of settling experiments was performed in the laboratory to examine the combined effects of suspension concentration and fluid-shear. A new settling function was proposed and compared to experimental results. Quiescent column-settling tests were performed over a range of concentrations, and a special particle-size settling test examined changes in dispersed particle-size distribution during settling.

Background

Fine, cohesive sediments occur as flocs in the environment. Flocs are loose aggregations of perhaps 10^6 individual particles. Floc-settling velocity is defined as the sinking rate in quiescent fluid. It affects vertical transport and distribution in the water column and maximum rate of deposition. Settling velocity of cohesive sediments varies with concentration and with fluid shear rate (Camp 1946; Krone 1962; Van Leussen 1989; and Kranck and Milligan, 1992).

Suspension concentration affects cohesive-sediment-aggregate collision frequency, floc size, and settling rate. For example, an empirical relation between median settling velocity and concentration can be developed from the results of Kranck and Milligan (1992): $W_s = 30.9\ C^{0.99}$ (mm/sec) where C is the total concentration in kg/m^3. Previous quiescent laboratory settling tests indicated $W_s \sim C^{4/3}$ (Krone 1962), and the difference in the exponent was

attributed to differences in turbulence conditions. Settling is enhanced from a lower concentration limit, C_{ll} typically 50 to 300 mg/l, to an upper limit, C_{ul} typically 1 to 10 g/l, at which particle interactions begin to hinder settling.

Fluid-shear promotes particle collisions and can, up to a point, promote floc growth. Since aggregate collisions and turbulence at the microscale can also break flocs apart (Camp 1946, Van Leussen 1989), only relatively low shear rates are effective at optimizing floc size. Specific data on the effect of shear rate on floc growth and settling are relatively rare for natural sediments. The measurements of Kranck and Milligan (1992) captured fluid-shear effects on floc characteristics in the field. Much work has been done on shear coagulation in waste water treatment (Camp 1946). Fluid-shear rate *G* has been termed root-mean-square velocity gradient, related to work input per unit volume per unit time and viscosity, and can be related to overall mean velocity and to overall turbulence intensity (McConnachie 1991). A multiplicative relationship that combined concentration and shear-rate effects on settling velocity was proposed by Malcherek and Zielke (1996). In the present notation that relationship is

$$W_s(gs) = a_1 \left(\frac{C}{C_{ul}}\right)^{n(gs)} \left(\frac{1 + a_2 G}{1 + a_3 G^2} \right) \tag{34}$$

for $C_{ll} \le C \le C_{ul}$, and where a_2 and a_3 are constants. Laboratory tests were performed and will be described in the remainder of this section.

Grain-size composition affects floc composition and settling, and, for the multiple-grain class model described in Chapter 6, some information is needed on the effect of grain size on floc settling rates.

Methods

Field settling tests were performed 18 to 20 June 1997 at four locations. A Niskin® water sampler tube with ball-valve end closures was used in the field tests. The sampler was lowered vertically to mid-depth, closed, and retrieved to the boat deck. The tube was sampled from a stopcock 430 mm below the upper sample surface for 20 min.

Experiments on the effects of both concentration and shear on settling velocity were performed in the laboratory. Tests were performed on a model clay and on resuspended estuarine-channel sediments. A model clay mixture was prepared from pure, dry clays. Dispersed particles greater than 10 μm Stokes settling were removed, and a stock mixture with 40 percent illite and kaolinite and 20 percent montmorillinite by dry weight was prepared. All three minerals were found by Whitehouse et al. (1960) and Edzwald et al. (1974) to flocculate at ionic concentrations lower than those used here. The stock mixture was allowed to stand a week after 15 ppt Instant Ocean salts were added. The clay stock mixture was mixed with 15 ppt artificial seawater to make test suspensions. A natural estuarine sediment from the GIWW channel about 11.2 km north of Port Isabel was also tested. This sediment had mean and median dispersed grain diameters of 26 and 7 μm, 7 percent sand (> 74 μm), and 64 percent less than 16

μm. The material had an *in situ* bulk wet density (*BWD*) of 1408 kg/m^3 and 8 percent organic content by weight.

Rotating flocculators were used to generate large flocs. Cylindrical flocculators 12.5-cm diameter by 21-cm long/deep were used to allow for settling velocity determinations after floc generation. Cylinders of 11.75-cm-diam by 28-cm-deep were used for two higher shear-rate and a quiescent settling experiment. For higher shear-rate model clay experiments, these cylinders were filled to 18-cm depth in a Particle Entrainment Simulator (PES). The PES is a standard device developed by Tsai and Lick (1986) that has a 2.5-cm-stroke oscillating grid.

The flocculators were filled, rotated such that the outside edge or wall moved at about 1 cm/sec for 3.5 to 7 hours until floc sizes stabilized, and then removed from the rotator, up-ended slowly to bring the axis to the vertical, and sampled over time with a pipette to determine floc settling velocities. In the first series of model-clay experiments, laminar shear rates were varied by partially filling the cylinders, and spanning those which produced maximum or optimum floc sizes. Shear rates were estimated visually by observing small particle movement at 5 to 10 locations in the disk flocculator. In the second series of model-clay experiments, only the optimum shear rate was used and compared to quiescent settling tests.

The quiescent cylinder experiments were conducted by mixing and introducing sediments and withdrawing samples from 20-cm depth for 6 hours. Care was taken to keep cylinders under constant temperature conditions. PES settling experiments were performed while grid oscillation was underway and producing mild turbulence. Oscillation rates at 70 and 140 per second produced estimated turbulent shear rates of about 20 and 40 per second. Estimations were made based on procedures presented by McConnachie (1991). The PES was operated at a rate below previous calibration range to produce mild turbulence and a shear stress of less than 0.05 Pa on the bed. Samples were withdrawn from 12.5 cm depth for 6 hours.

Two series of tests were performed on the natural sediment: one using rotating cylindrical flocculators and the other in a 10-cm-diam by 1.9-m-high column. The disk flocculator, operated at the shear rate found to be optimum for the model clay, produced large flocs. Photo-micrographs and grids were used to visually estimate floc dimensions, which were found to vary between < 0.2- and 0.8-mm-diam, depending on the test. Samples were analyzed for total suspended material, and median settling velocities were estimated.

A special column experiment was made specifically to examine the change in dispersed particle size during settling. During this quiescent column test, four large-volume samples were collected for size analysis. Cumulative and differential size and settling velocity distributions were calculated. A Coulter LS 100Q® instrument was then used to determine particle size in 128 channels from 0.4 to 1000 μm. This instrument uses laser near-forward scattering to estimate particle size.

Results

Field settling tests had low initial TSM values that fell within a narrow range, as summarized in Table 25.

Table 25
Field Settling Tests June 1997

Date	Station	Initial TSM, mg/l	Median W_s , mm/sec
6/18/97	OBS/b6	51	0.13
6/19/97	Baffin/b7	29	0.12
6/20/97	LLM3.5/b7	28	0.33
6/20/97	LLM3.7/b10	74	0.32

Station locations are given in Table 14 of Chapter 3.

The effects of shear rate G alone on settling are shown in Figure 38 for model clay suspensions with initial concentrations of 46 mg/l. Also shown is a fit to Equation 34 with W_{s_o} set to a constant equal to the median W_s value observed in the corresponding quiescent test. The median W_s for the quiescent test was about the same with a G value of about 30 Hz. The maximum floc settling rates were more than 100 times greater than with $G = 0$. They occurred at a very low shear rate (about 0.5 Hz) and dropped off sharply with increasing G.

Results on the effects of concentration and shear rate on W_s for model clay and natural sediments are shown in Figures 39 and 40. Test data are $W_{s_{50}}$'s for disrupted floc (quiescent tests which began with floc disruption) and for optimum flocs ($G = 0.5$ Hz). The model clay-floc settling velocity decreased as initial concentration increased from 57 to 196 mg/l (Figure 39). Eleven floccculator tests were performed with the natural sediment over a concentration range of 60 to 660 mg/l at $G = 0.5$ Hz (Figure 40). There was a slight upward trend in the linear regression line between initial concentration and median W_s , but the slope was not statistically different from zero. Nine quiescent column tests were performed between initial concentrations of 72 and 1,012 mg/l (Figure 40). Above 122 mg/l median W_s's increased steadily, indicating that suspension concentrations were not hindering settling and were generally in the range of $C_{ll} \le C \le C_{ul}$. Optimum-floc and disrupted floc W_s *'s* matched at about 500 mg/l (Figure 40). Therefore, contrary to Equation 34, floc settling rates did not increase with concentration in either model clay or natural sediment tests.

Based on experimental results, the effects of concentration and shear rate on settling velocity are not taken to be multiplicative as in Equation 34, and the following functional relationship is proposed:

$$W_s(gs) = a_1 \left(\frac{C}{C_{ul}}\right)^{n(gs)} \left(\left(\frac{1 + a_2 G}{1 + a_3 G^2} \right) \exp(-a_4 C/C_{ll}) + 1 \right) \qquad (35)$$

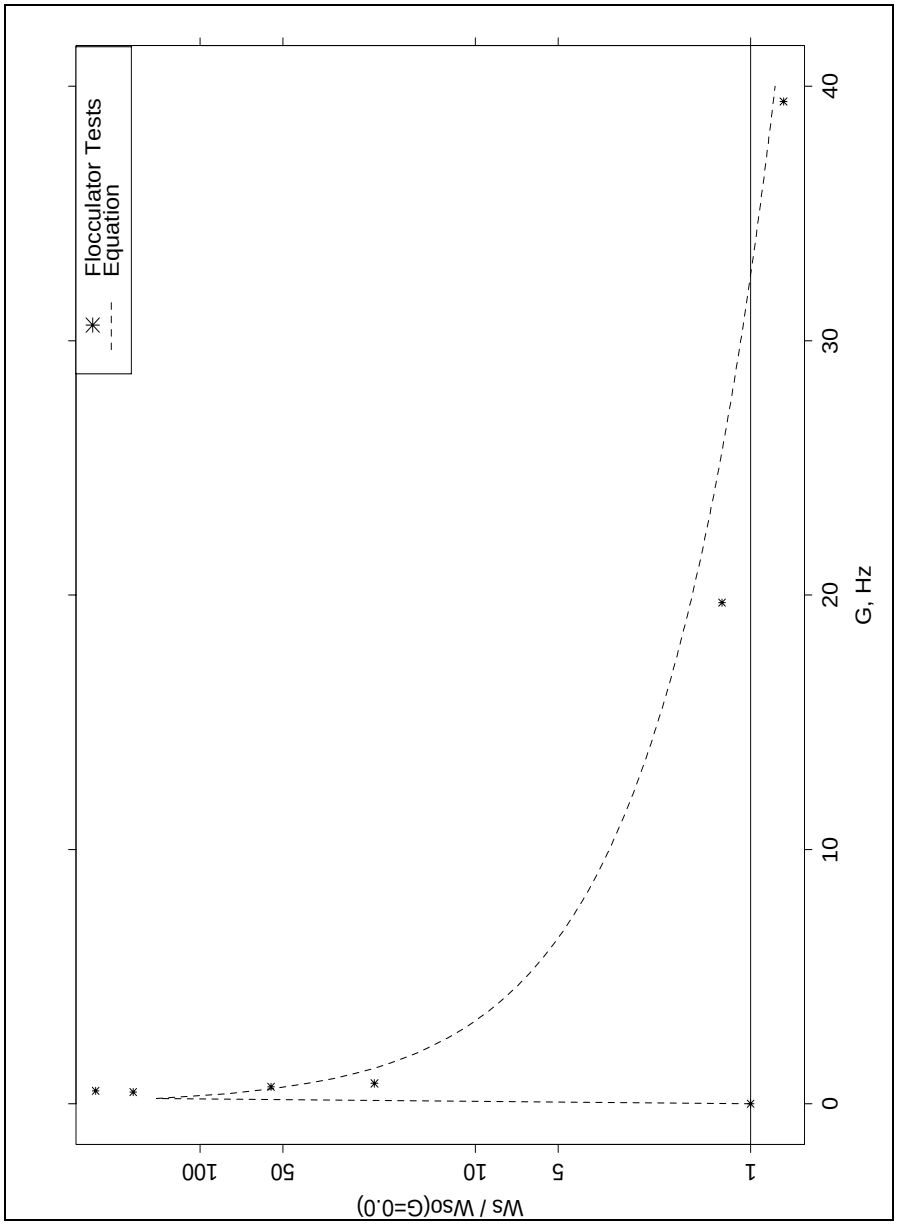

Figure 38. Experimental results for the effect of shear on settling velocity and a fit of Equation 34 to the data

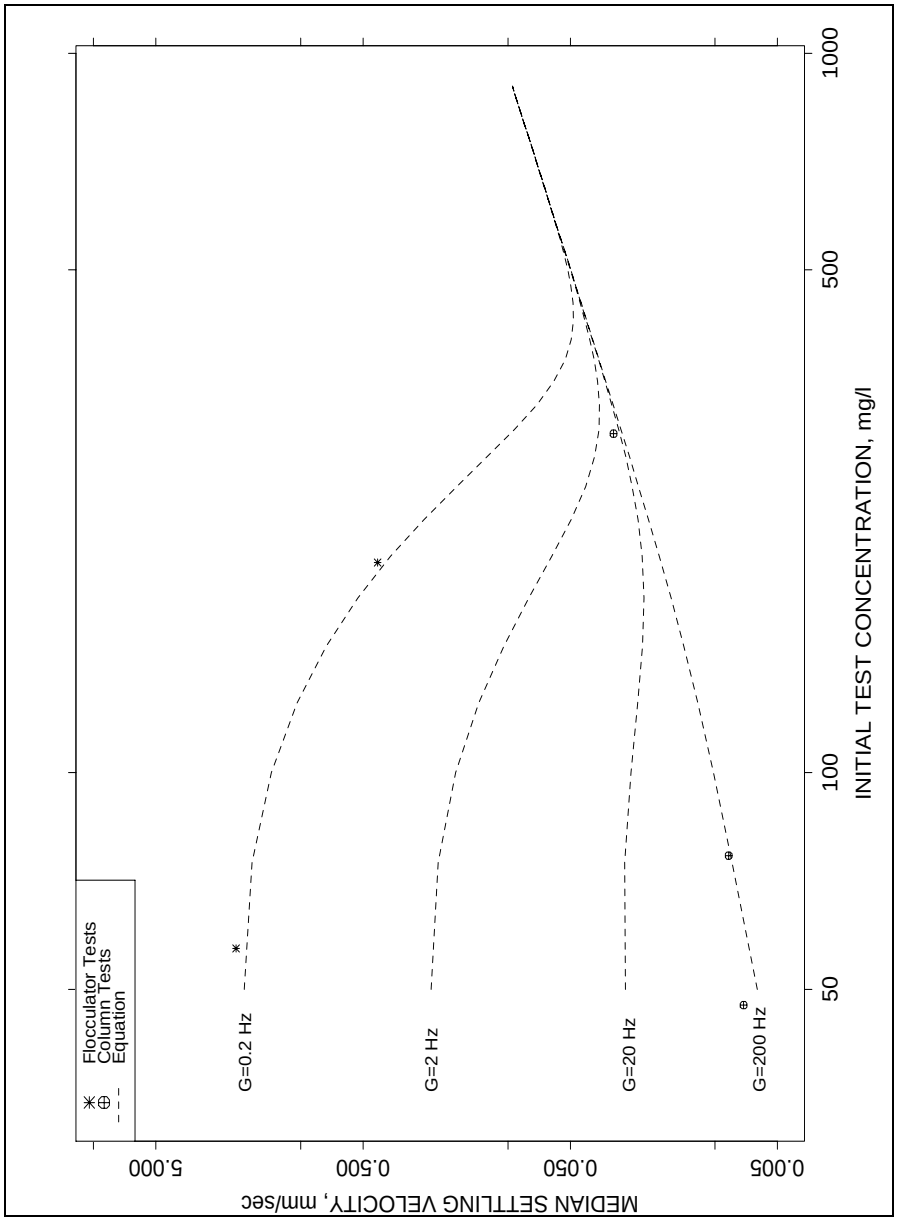

Figure 39. Model clay settling velocity results for varying shear and concentration and a fit of Equation 35 to the data

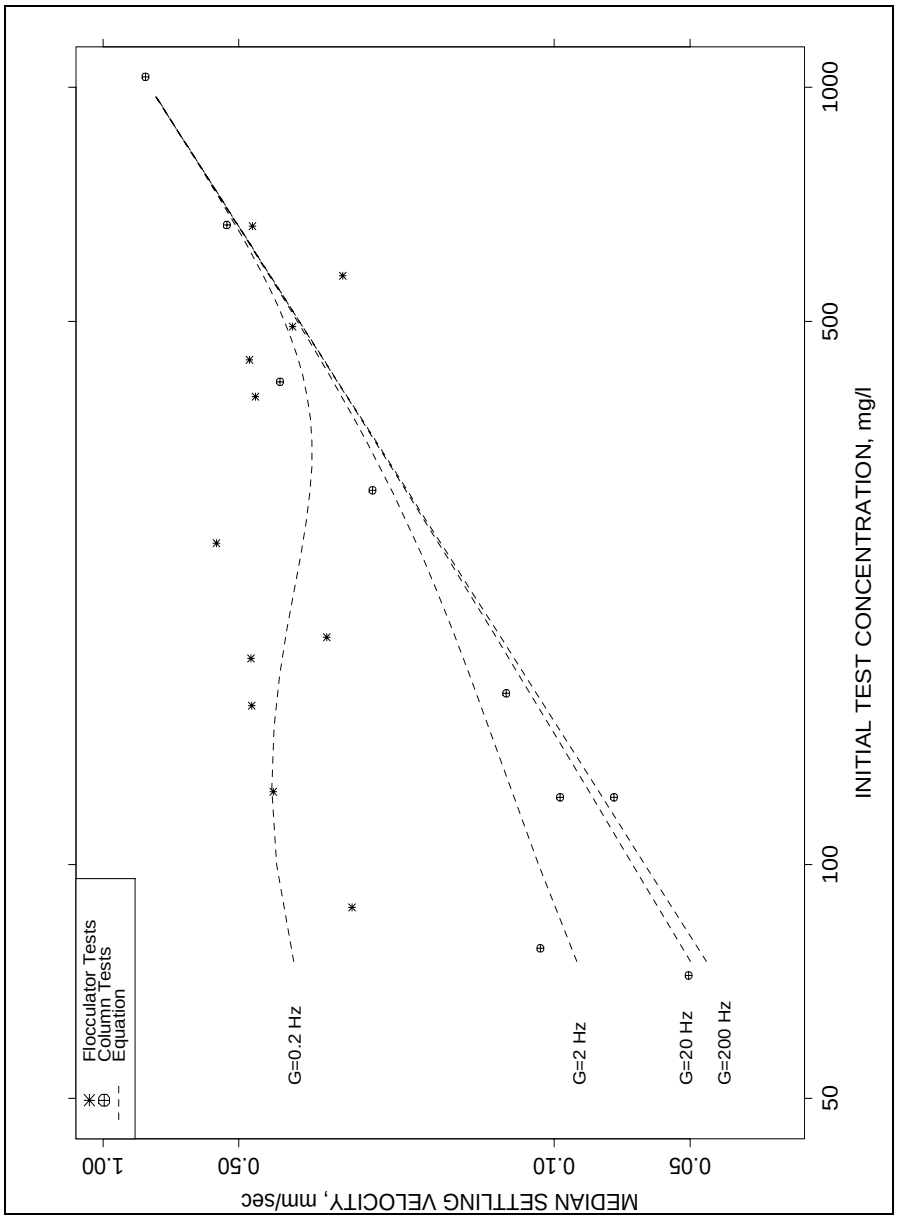

Figure 40. Natural sediment settling velocity results for varying shear and concentration and a fit of Equation 35 to the data

for $C_{ll} \leq C \leq C_{ul}$. Equation 35 is shown plotted in Figures 39 and 40 as approximate fits to the data.

The cumulative dispersed particle size and floc-settling velocity distributions for the special particle-size settling test are shown in Figure 41. The settling velocity distribution is narrower or better sorted than the dispersed particle-size distribution due to flocculation. The 25, 50, and 75 percentiles for this quiescent settling test (initial concentration of 660 mg/l), along with other tests in series, are plotted in Figure 42 and presented in Table 26. Spread of settling velocity distributions is only slightly narrower at higher concentrations. Differential dispersed particle-size distributions for 0 to 60 min of a column settling test are shown in Figure 43 as absolute concentration by size channel. This plot shows how various particle sizes settled from suspension. Median settling velocities were calculated for certain dispersed particle sizes that correspond to dectiles on the cumulative dispersed particle-size distribution. Results are shown in Table 27. As described earlier, particles settle not as individuals but as flocs. Figure 43 demonstrates that the largest dispersed particle sizes settled from the suspension most quickly, and, therefore, flocs containing the largest dispersed particles settle fastest.

Table 26
Settling Velocity Distribution, mm/sec, for Quiescent Column Tests

Initial TSM, mg/l	75 Percent Less Than	50 Percent Less Than	25 Percent Less Than
166	0.27	0.13	0.06
303	0.56	0.25	0.09
418	0.57	0.40	0.17
665	0.89	0.55	0.35
1,032	1.50	0.75	0.46

Table 27
Settling And Dispersed Particle Size Distributions

Percent Less Than	Cumulative Settling Velocity, mm/sec	Cumulative Dispersed Particle Size, μm	Discrete Settling Velocity for Cumulative Size, mm/sec
90	1.495	34.3	0.708
80	0.976	19.3	0.598
70	0.760	10.0	0.559
60	0.637	5.8	0.508
50	0.555	3.9	0.473

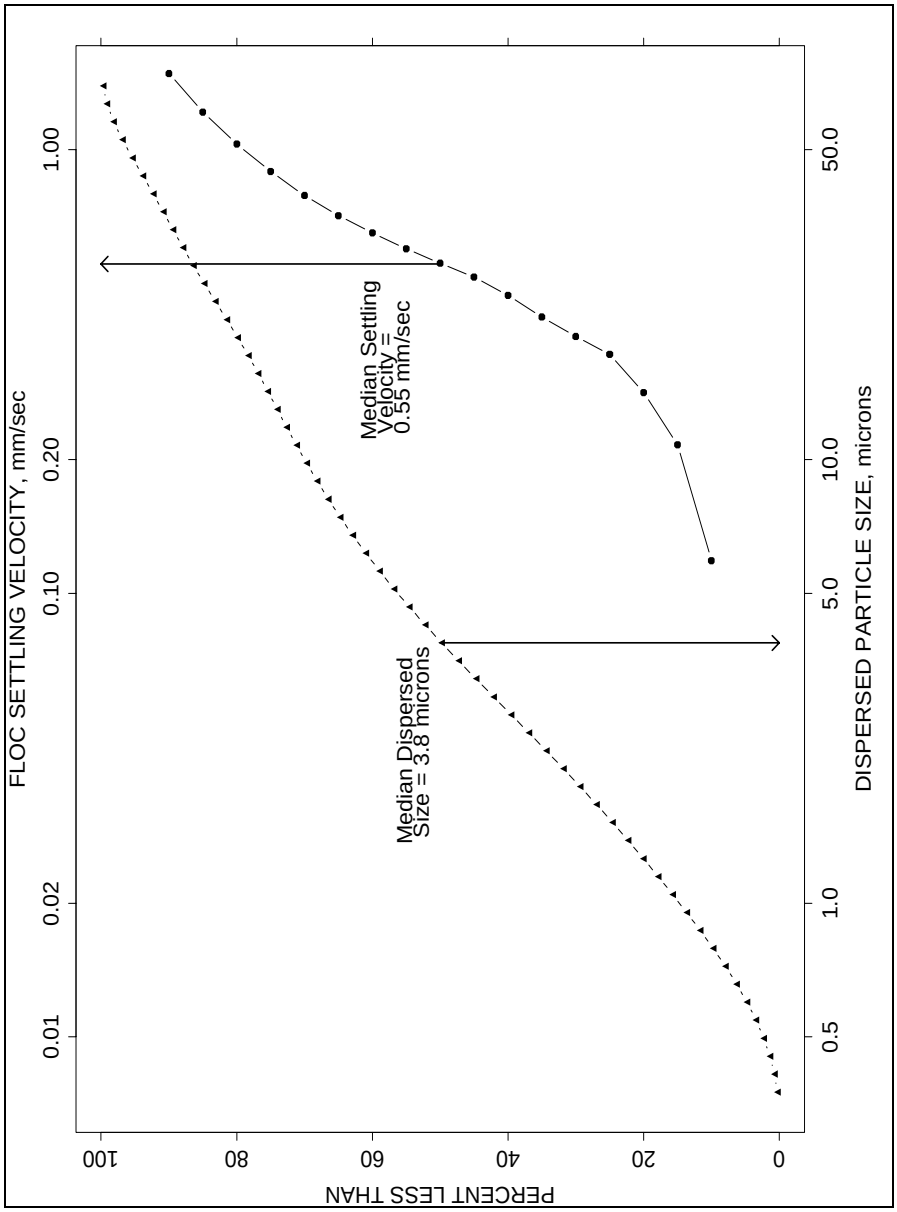

Figure 41. Cumulative settling velocity and dispersed particle-size distributions for the special particle-size settling test

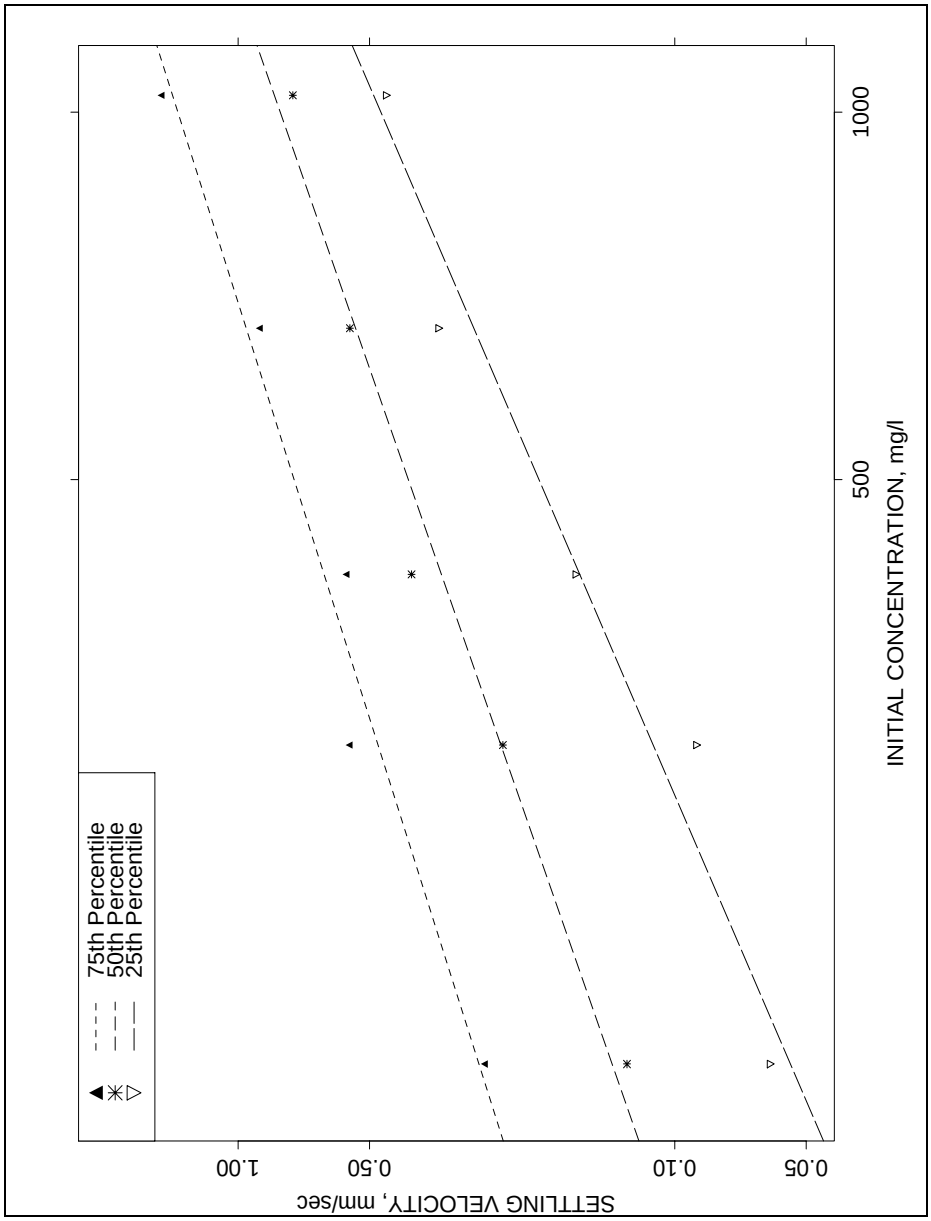

Figure 42. The 25, 50, and 75 percentile (less than) settling velocities for quiescent column tests

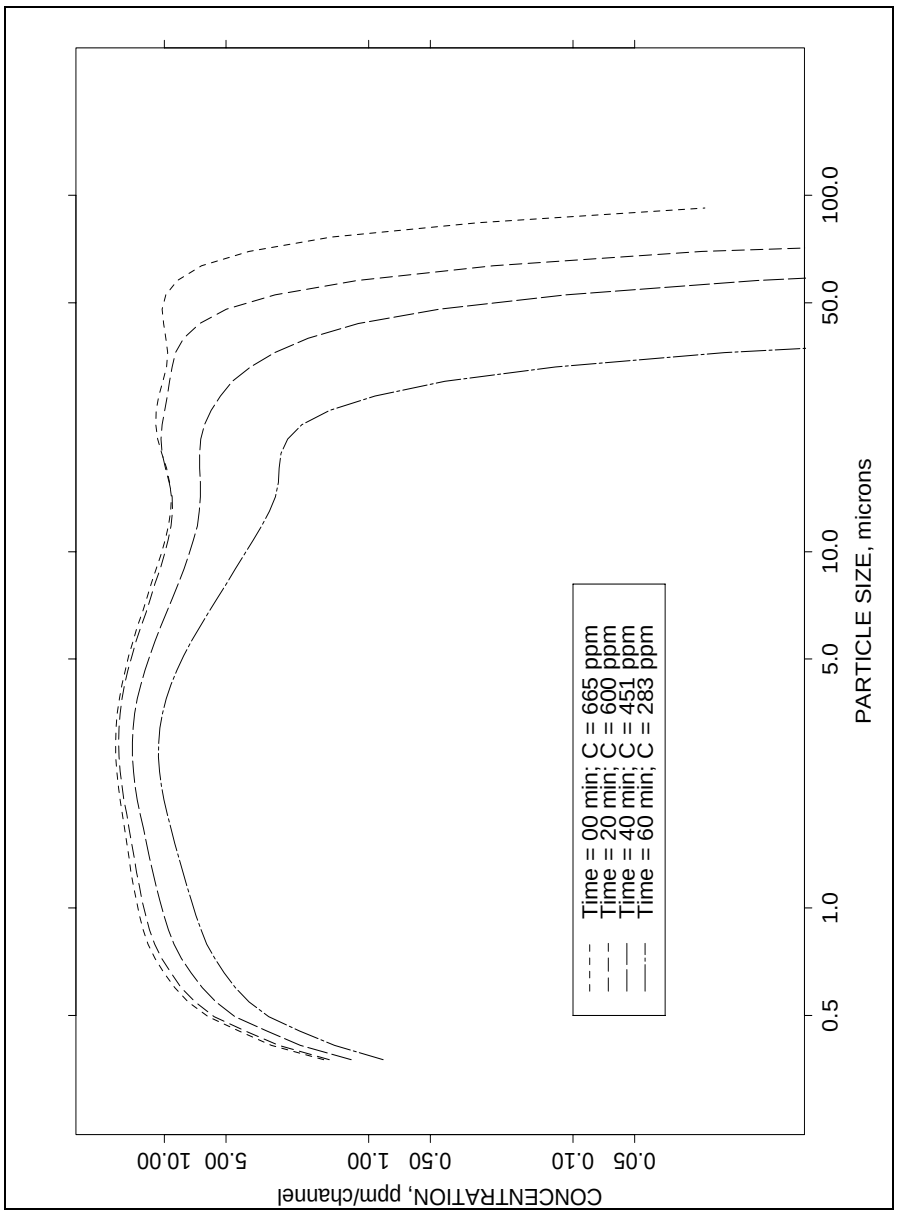

Figure 43. Time-series of discrete dispersed-particle-size distributions during the special particle-size settling test

Bed Sediments

Methods

Bed samples were collected with a push-corer or a box corer, depending on water depth and the purpose of the sample. Most samples were collected with a 3.8-cm-ID, clear PVC push corer. A flap valve above the push core barrel maintains suction as the sample is withdrawn from the sediment bed. On deck, the core was subsampled as it was extruded from the core barrel. Samples were stored in labeled and doubled zip-lock bags. A square, 15-cm stainless steel box corer manufactured by Wildlife Supply Co.® was used for sampling the bed in deeper areas such as the GIWW channel and for use in erosion experiments.

Samples were analyzed to determine bulk wet density with 25-cm^3 pycnometers. Salinity was determined using an AGE Autosal® instrument, and calculated by conversion from density, determined with a PARR® densitometer. Organic content was determined as the dry weight loss on ignition after 1 hour at 550 °C. To determine particle size-distribution, sediment samples were first cleaned with Clorox® washings (oxidation) and acetone washings (removal of hexane soluble material), to remove organics, and dispersed with Calgon®. Additional washings with sodium carbonate/bicarbonate were made after the oxidation steps. A Coulter LS 100Q® instrument was then used to determine particle size. Subsamples were stored at 4 °C prior to testing.

An electrical resistivity probe was also used to profile sediment density. The probe was built by Dr. R.F. Corwin, Consulting Geophysicist, of El Cerrito California for the WES. The electrodes and body of the probe are hardened brass tubing, 1.9-cm OD. A pressure-proof case carries pressure, temperature, and tilt sensors. Two electrodes transmit a 100-Hz square-wave signal regulated to 100 mA. The signal is received through the other two probe electrodes. Response time is about 0.035 sec for 95 percent response. Material less than 0.2 or greater than 5 cm from the electrodes does not affect the signal. In theory

$$R = K(V/I) \tag{36}$$

where R is resistivity in ohm-cm, K is a probe constant, V is signal voltage, and I is current. The bulk wet density BWD in g/cu cm of the sediment is linearly related to resistivity by

$$BWD = 0.388F + 0.634 \tag{37}$$

where F is the formation factor or ratio between R in the sediments to the resisitivity R_o just above the sediment bed ($F = R / R_o$).

Results

The DGPS locations of the bed material sampling are given in Table 28.

Table 28
Bed Sediment Station Locations

Date	CST	Station	Latitude N	Longitude W
12/09/96	1229	b0	26°-10.8862'	97°-15.2327'
12/09/96	1153	b1	26°-10.9703'	97°-15.0318'
12/09/96	1237	b2	26°-10.8447'	97°-15.3663'
12/09/96	1307	b3	26°-10.7578'	97°-15.6017'
12/09/96	1400	b4	26°-08.3660'	97°-15.6523'
12/09/96	1400	b5	26°-06.3967'	97°-15.6067'
6/18/97	1545	b6	26°-10.9216'	97°-15.2739'
6/19/97	1509	b7	27°-11.5129'	97°-25.7059'
6/20/97	1017	b8	26°-35.3991'	97°-22.9373'
6/20/97	1208	b9	26°-36.0581'	97°-25.8178'
6/20/97	1335	b10	26°-33.6663'	97°-25.0518'
6/21/97	0953	b11	26°-08.0838'	97°-12.4498'
6/21/97	1111	b12	26°-13.2478'	97°-16.0671'
6/21/97	1127	b13	26°-10.9020'	97°-15.2130'
11/09/97	1311	b14	26°-06.1672'	97°-12.9316'
11/09/97	1400	b15	26°-06.8175'	97°-13.3745'
11/09/97	1422	b16	26°-07.3031'	97°-13.6312'
11/09/97	1432	b17	26°-07.7734'	97°-13.6312'
11/09/97	1451	b18	26°-08.4049'	97°-14.2365'
11/09/97	1500	b19	26°-08.9326'	97°-14.4873'
11/09/97	1510	b20	26°-09.4671'	97°-14.7524'
11/09/97	1520	b21	26°-09.9399'	97°-14.9215'
11/09/97	1537	b22	26°-09.4823'	97°-14.7051'
11/09/97	1547	b23	26°-08.9982'	97°-14.3662'
11/09/97	1600	b24	26°-08.4942'	97°-14.1068'
11/09/97	1622	b25	26°-07.9026'	97°-13.5927'
11/09/97	1632	b26	26°-07.3786'	97°-13.2991'

Date	CST	Station	Latitude N	Longitude W
11/09/97	1645	b27	26°-06.8474'	97°-13.0056'
11/09/97	1655	b28	26°-06.3527'	97°-12.7212'
11/13/97	1549	b29	26°-33.8502'	97°-24.0738'
11/13/97	1554	b30	26°-34.1165'	97°-24.1038'
11/13/97	1600	b31	26°-34.4852'	97°-24.1538'
11/13/97	1608	b32	26°-34.7717'	97°-24.1764'
11/14/97	0827	b33	26°-04.9686'	97°-15.0636'
11/14/97	0840	b34	26°-06.1404'	97°-16.9780'
11/14/97	0842	b35	26°-06.1027'	97°-16.9793'
11/14/97	0902	b36	26°-08.2269'	97°-16.5566'
11/14/97	0924	b37	26°-11.7327'	97°-15.8034'
11/14/97	0933	b38	26°-11.6539'	97°-15.6861'
11/14/97	0942	b39	26°-11.6760'	97°-15.6251'
11/14/97	0947	b40	26°-11.8500'	97°-15.6692'
11/14/97	0952	b41	26°-12.0260'	97°-15.6986'
11/14/97	0957	b42	26°-12.2131'	97°-15.7448'

Table 29 summarizes laboratory measured *BWD*'s , station depths *h,* and particle size characteristics.

Table 29
Summary of Bed Sediment Density and Grain Size Measurements

Station	*h*, m	*z*, m	*BWD*, kg/m^3	D50, µm	%< 4 µm	%< 16 µm	%< 74 µm
b0	3.7	0-0.12	1369	7	38	64	93
b1	1.2	0-0.05	1746	207	3	5	7
		0.4-0.45	1933	37	23	37	63
b2	1.0	0-0.05	1688	174	7	12	21
		0.4-0.45	1895	18	31	39	66
b3	1.0	0-0.05	1814	127	3	5	13

Station	*h*, m	*z*, m	*BWD*, kg/m^3	D50, µm	%< 4 µm	%< 16 µm	%< 74 µm
		0.4-0.45	1466	18	28	48	69
b4	1.4	0-0.05	2056	160	7	10	19
		0.4-0.45	1197	35	25	39	69
b5	1.4	0-0.05	1861	118	11	13	31
		0.4-0.45	1711	60	26	44	54
b6	1.7	0-0.09	1949	205	3	4	8
b7	2.0	0-0.09	1379	138	16	24	31
b8	1.0	0-0.05	1868	227	4	6	8
b9	2.0	0-0.05	1920	193	2	3	5
b10	1.5	0-0.05	2159	155	18	27	33
		0-0.09	1826	21	31	48	57
b11	-	0-0.05	1764	-	-	-	-
b12	4.3	0-0.09	1301	6	42	69	91
b13	3.0	0-0.09	1868	11	32	54	80
b14	-	0.09-0.12	1820	39	27	40	59
b17	1.2	0.12-0.15	1778	23	29	45	68
b24	0.8	0-0.06	1451	144	7	10	27
		0.12-0.15	1825	171	8	11	24
b28	0.9	0-0.06	1751	75	9	16	50
		0.12-0.24	1858	28	28	44	65
b31	1.7	0.15-0.18	1949	260	3	4	6
b33	0.6	0-0.06	1900	162	2	3	5
b34	1.1	0-0.06	1757	4	51	81	99
b36	0.6	0-0.05	1910	144	6	9	17
		0.3-0.33	1794	17	33	49	69
b37	0.9	0-0.05	1922	133	6	9	19
		0.37-0.4	1670	148	17	26	35
b38	1.1	0-0.02		4	51	76	99

Resistivity measurements were collected in November 1997 in Lower Laguna Madre west of the GIWW channel on the fringes of dredged-material placement areas. Measurements from many of these stations matched those of stations where bed samples had been collected and the results reported in the last section. Results for two depths in the sediment bed z_o and z from the resistivity probe are summarized in Table 30. The location z_o was the nearest measurement to the sediment-water interface.

Table 30
Summary of Resistivity Measurements on Bed Sediment

Station	h, m	z_o , m	BWD, kg/m^3	$\underline{z}$, m	BWD, kg/m^3
b14	-	0.03	2024	0.04	1853
b15	1.1	0.03	2043	0.07	1952
b16	0.9	0.03	1988	0.03	1982
b17	1.2	0.03	1640	0.15	1510
b18	1.2	0.03	1520	0.06	1480
b19	1.1	0.03	1760	0.03	1760
b20	1.0	0.03	1440	0.03	1440
b21	1.2	0.03	2020	0.23	1460
b22	1.0	0.03	1620	0.04	1600
b23	1.2	0.03	1620	0.11	1520
b24	0.8	0.03	1900	0.03	1900
b25	1.0	0.03	1710	0.24	1530
b26	0.9	0.03	1620	0.29	1490
b27	0.9	0.03	1520	0.06	1480
b28	0.9	0.03	1790	0.06	1740
b29	1.0	0.03	1920	0.14	1720
b30	-	0.03	1190	0.36	1120
b31	1.7	0.03	1640	0.08	1380
b32	1.5	0.03	1930	0.04	1910
b35	1.2	0.03	1760	0.2	1620
b36	0.6	0.03	1980	0.26	1410

Station	h, m	z_o , m	BWD, kg/m^3	$\underline{z}$, m	BWD, kg/m^3
b37	0.9	0.03	1590	0.29	1210
b38	1.1	0.03	1540	0.39	1420
b39	1.1	0.03	1530	0.24	1330
b40	1.2	0.03	1540	0.39	1260
b41	1.0	0.03	1550	0.28	1310
b42	1.1	0.03	1510	0.36	1270

Erosion Experiments

Laboratory erosion experiments were conducted on sediments to support numerical model predictions of short-term dredged-sediment dispersion. Sediments were undisturbed box-core samples and composites from Laguna Madre. Test sediments were generally cohesive and had substantial clay-, silt-, and sand-size fractions. Before erosion testing, channel sediments were slurried to simulate the effects of hydraulic dredging and disposal operations during which sediments would be sheared and mixed with water. Slurried sediments were mixed with site water to form 4-cm-thick layers, allowed to settle up to 27 days, and erosion tested without further disturbance. Test matrices of 3 to 4 initial slurry densities and 4 to 5 standing or resting times were performed on each channel sediment. Estimates of average layer densities at test times were based on layer thicknesses. Surface erodibility decreased most rapidly during the first days after slurrying and never reached the erosion resistance of the original channel sediments. A surprising result was that erodibility was more poorly correlated to average test density than to standing time. Some sediment samples were erosion tested at 10 °C and/or settled at 6 °C to gage the effect of temperature on these processes. Linear and nonlinear erosion models, with and without erosion thresholds, were fit to the data, and information was used in a multiple-grain class numerical sediment model.

Background

Cohesive dredged sediments disposed in open water settle and increase in density with time. Since hydraulic shear strength has been found to be a strong function of density (Owen 1970; Thorn and Parsons 1980; Nicholson and O'Connor 1986; Teeter 1987), erodibility can be expected to change with time as well. Cohesive sediment density is often used to characterize a given sediment's erodibility. The erosion rate E at a given shear stress or the threshold shear stress for erosion τ_{ce} are indicators of erodibility. For example, expressions are used in models in the form: $E \propto \rho^{n1}$ or $\tau_{ce} \propto \rho^{n2}$ in which $n1$ and $n2$ are empirical exponents and ρ is some deposit density parameter such as volume concentration, porosity, dry-solids content, etc.

Cohesive sediments are thixotropic, and rheological properties change with time (van Kessel and Bloom 1998). Sheng (1994) and Johansen et al. (1997) found that deposit age had a pronounced effect on erodibility. Other sediment and pore-fluid characteristics affect erodibility. One purpose of these erosion tests was to identify and quantify important parameters controlling the erodibility of newly-deposited dredged material.

Accurately predicting fine-grained sediment erosion is difficult, and erosion tests were performed to simulate field conditions and to provide information to support various engineering assessments, including numerical sediment modeling of the post-disposal dredged material. In this study, sediments were slurried to various degrees in the laboratory and allowed to settle under controlled conditions to simulate dredging and disposal. The degree of slurrying or dilution ratio, deposit age, density, grain mixture, and temperature were investigated as factors controlling deposit erodibility. This section describes experimental procedures, results, and erosion model comparisons based on analysis of erosion experiment results.

Materials and methods

Experimental material was obtained from Lower Laguna Madre with a WILDCO® 15-cm box core. Sub-samples were taken for bulk wet density (*BWD*), salinity of interstitial water, organic content, and particle size distribution in accordance with the same laboratory procedures described in an earlier chapter.

Four series of erosion experiments were performed. The first test series consisted of six bay-sediment tests from bare areas of Lower Laguna Madre. Samples b1 to b5 were collected in 1996 near the CBI FIX stations and along the axis of the deep, bare area between the FIX stations and Port Isabel. Sample b6 was collected in June 1997 from the area of the FIX stations. Station locations are given in Tables 11 and 14. Separate sediment characterization tests were performed on the experimental sediments.

The second series of tests was performed on Lower Laguna Madre channel-sediment sample b0 slurried 1:3 and 1:4 (sediment : water) and settled 1 to 27 days. Eight erosion experiments were performed in this series. The third test, b12, was a channel sample slurried 1:3, settled 2 to 10 days, and tested at 23 °C and 10 °C . The third test series was an attempt to examine the effect of temperature on erodibility.

The fourth test series was performed on a composite sediment made from channel material (b0 and b12) and material from the sandy area of the bay (b1 to b5) west of the channel. This sediment mixture was more representative of material remaining in placement areas after some erosion has taken place. The fourth series consisted of three slurries mixed 1:1, 2:1, and 5:1 (sediment : water). Initial slurry densities were 1206, 1268, and 1329 kg/m^3 , and each was tested after 1, 7, 14, and 21 days (12 total tests).

Erosion experiments were carried out in a Particle Entrainment Simulator (PES), a portable device proposed by Tsai and Lick (1986) and used extensively for testing undisturbed core sections. The WES PES has an erosion chamber geometry identical to that used by several other investigators and is intended primarily as a field tool for erodibility assessment of undisturbed 11.75-cm-diamr cohesive-sediment core sections. An oscillating grid in the PES generates turbulence above sediment to simulate the erosive shear stress of a shear flow, and, therefore, mean bed shear stress, normally used to correlate erosion, is not available as a measurable parameter. The PES was originally calibrated by the comparison of test suspension concentrations to those from an annular flume. The original calibration was used to correlate oscillation rates to an equivalent shear stresses. During low-temperature erosion tests, a water chiller was used to circulate water through a copper coil wrapped around the erosion chamber to maintain low temperatures.

Equivalent shear stresses were increased step-wise during erosion tests and the concentration of suspensions were monitored with time. PES tests started with an initial 2-min period at 100 rpm, or less than 0.1 Pa, to suspend very loose sediment that might result from the bed preparation. The equivalent shear stresses were then typically stepped up to 0.2, 0.3, 0.4, and 0.5 Pa allowing 30 min at each step.

The level of the sediment interface or surface was measured immediately after preparation and before each erosion test. The volume concentration *Cv* and *BWD* after standing were estimated at test time by taking the ratio of the initial- to the settled-sediment thicknesses and multiplying by the initial slurry *Cv*.

Suspended samples of 30 ml were withdrawn from the erosion chamber for filtration. Particle-free water was introduced during sampling to keep the water level constant in the PES erosion chamber. Samples of suspensions were analyzed to determine the mass of sediments eroded from bed surfaces. Samples were filtered through 0.45 μm pore-size polycarbonate Nuclepore® filters to determine total suspended material. Because the suspension volume of the PES is relatively small, the PES suspension concentrations were adjusted for the mass withdrawn during sampling. An adjustment equal to the calculated decrease in concentration due to sampling and chamber replenishment was added to the results of subsequent samples.

Each shear-stress step was analyzed by regression analysis to determine erosion rate *E*. Acceleration effects early in shear-stress steps added a time-varying component to *E*. To avoid these effects, regressions were performed on adjusted concentrations from 10 to 30 min into each step. Regression results were deemed acceptable if p-values were less than 0.20. This procedure eliminated some results with near-zero slopes and/or marginal regression fits.

Critical or threshold shear-stress for erosion was determined by the regression of shear stress against *E* . Analysis of variance (AOV) was performed with *E* as the response and standing time or deposit age and deposit wet density both grouped or nested by shear-stress level.

Results

Example erosion test time series for the first and second test series are shown in Figures 44 and 45.

Characterization results for the sediments are given in Table 31.

Table 31
Erosion Test Sediment Characteristics

Test Series	*BWD*, kg/m^3	LOI, % by wt.	Salinity, ppt	Sand, % by wt.	Mean size, µm	Mode size, µm	Median size, µm
2	1308	8.2	34.0	7	25.8	3.7	7.1
3	1301	9.0	34.2	1	12.0	3.0	4.3
4	1390	4.4	33.4	45	127.2	(a) 3.5 (b) 203	107.5

The sediment used in series 4 was a bimodal mixture of channel and sandy bay sediments described earlier and was not an *in situ* material.

AOV on data from the third test series indicated that, for Laguna Madre channel sediments, deposit age, or standing time, was a significant factor controlling E (p-value < 0.01), while deposit density was not significant (p-value = 0.77). The same result was found for the fourth test series on Laguna Madre mixed sediment. Initial slurry density was likewise not a significant factor for E, even though the fourth test series had the greatest range of initial slurry densities. Linear-regression fits through 1-, 7-, 14-, and 21-day standing time, taking all slurry tests together, are shown in Figure 46. Cumulative probability distributions for these standing times, plotted on standard deviation coordinates, are shown in Figure 47. Distributions of these data and other test series were about log-normal. Data from the fourth test series plotted by initial *BWD* as probability distributions are shown in Figure 48. Distributions were similar and statistically equivalent.

Discussion

The most significant factor, other than shear stress, affecting erosion rate E of slurried channel muds was standing time, or deposit age, (p-values < 0.01). Initial slurry density or density at the time of the erosion experiments was not significant for Laguna Madre sediments. Since cohesive bonds are what give muds hydraulic shear strength, bond formation appears to be a thixotropic effect that requires many weeks to complete. Deposit density is an indicator of the proximity of particles to one another, but not a good indicator of cohesive bonding, except perhaps at very long standing times.

Standing time was found to be better correlated to erosion rate, erosion threshold, and erosion constant than sediment density. Various erosion models, with and without erosion thresholds, were fit to the data: the former a somewhat better fit the data. Erodibility was equivalent for 10 and 22 °C temperatures, but reduced temperature decreased standing and consolidation.

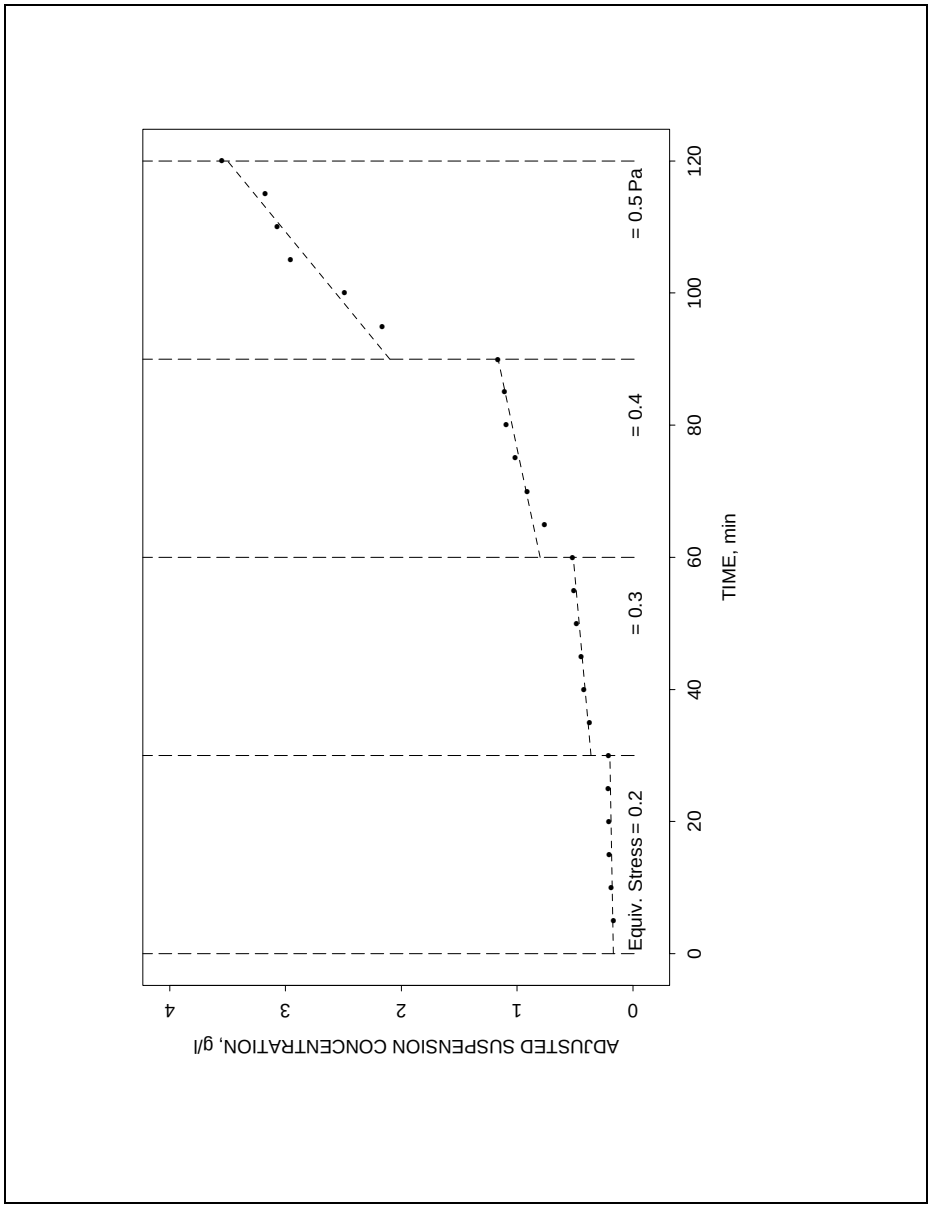

Figure 44. Example suspension time-series for sample b4 of the first test series

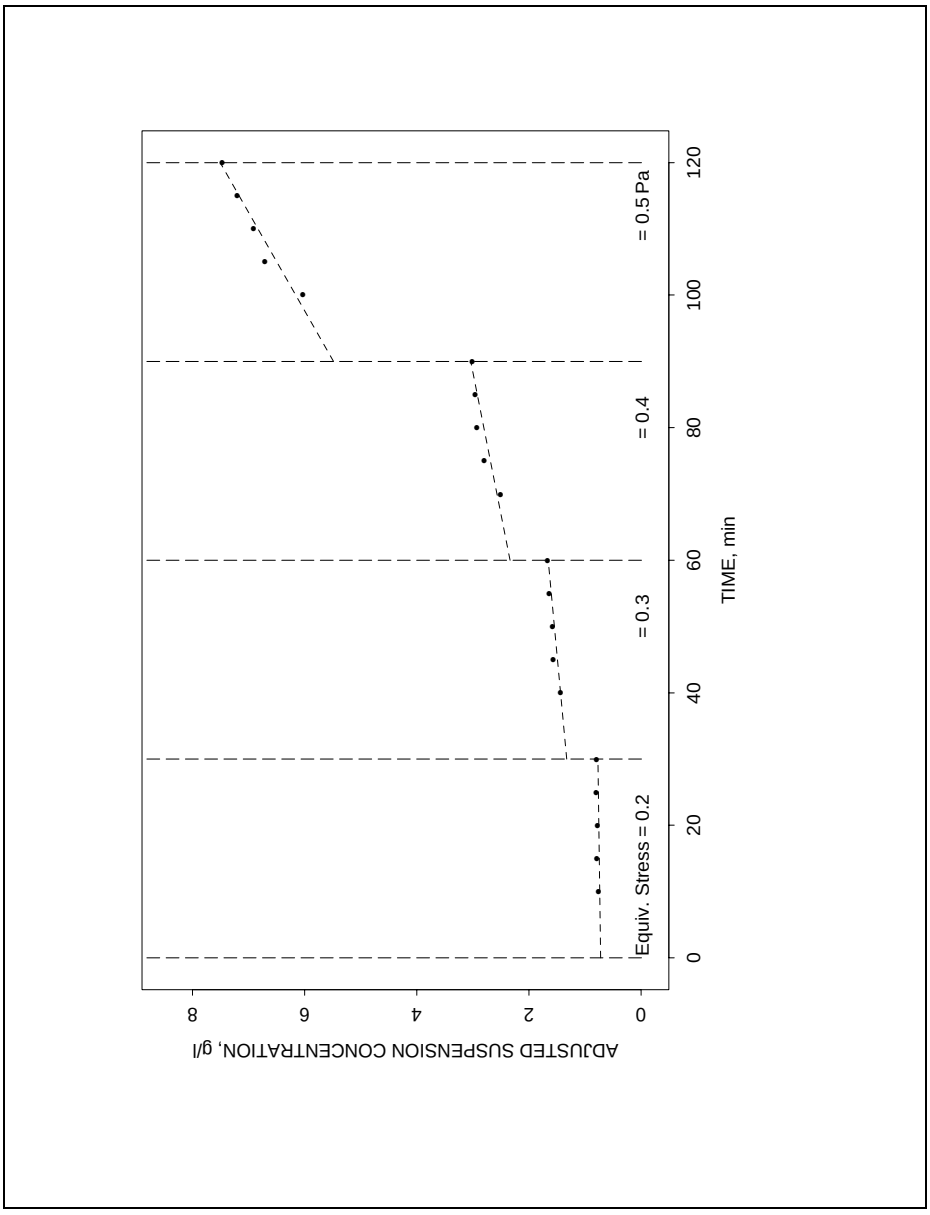

Figure 45. Example suspension time-series for 7-day standing time in the second test series

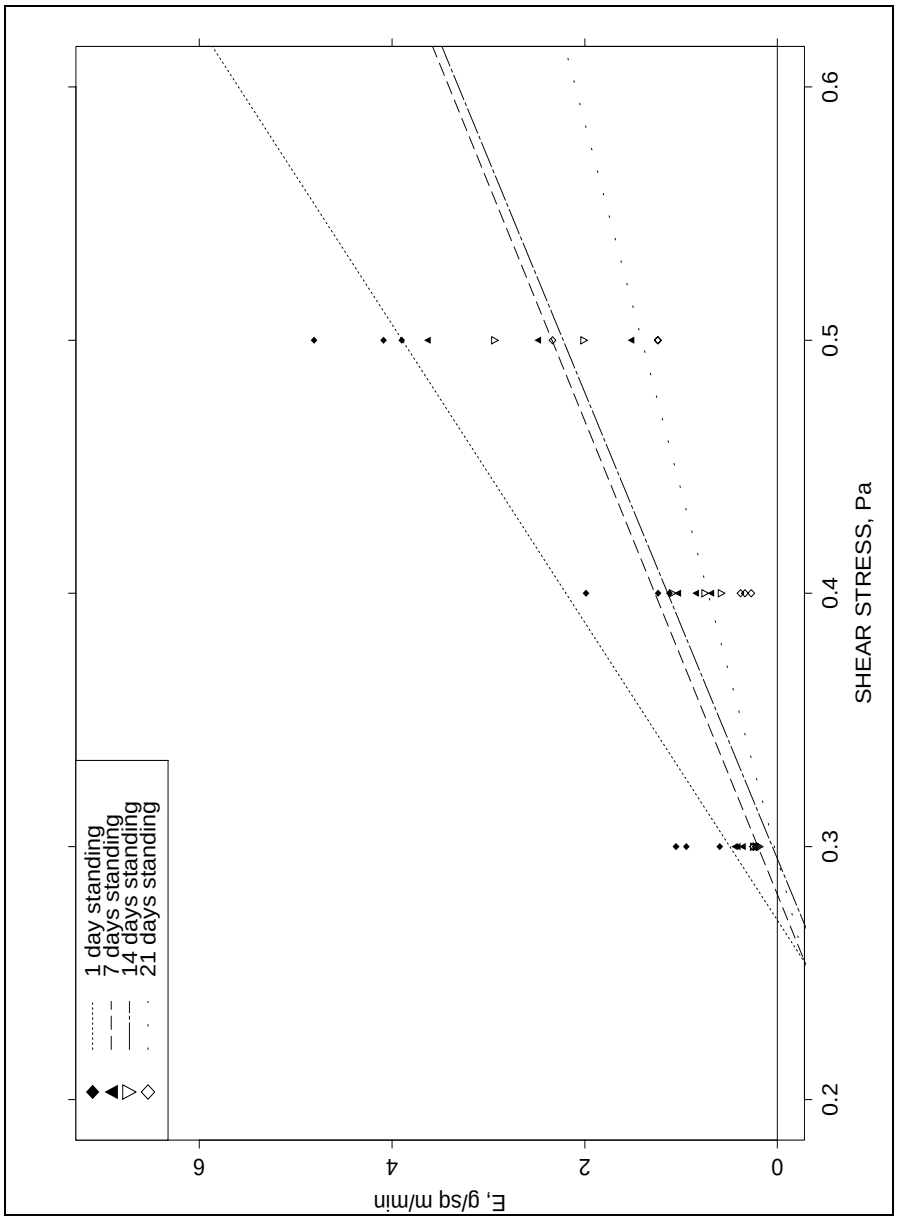

Figure 46. Linear-regression fits through 1-, 7-, 14-, and 21-day standing time taking all slurry tests together

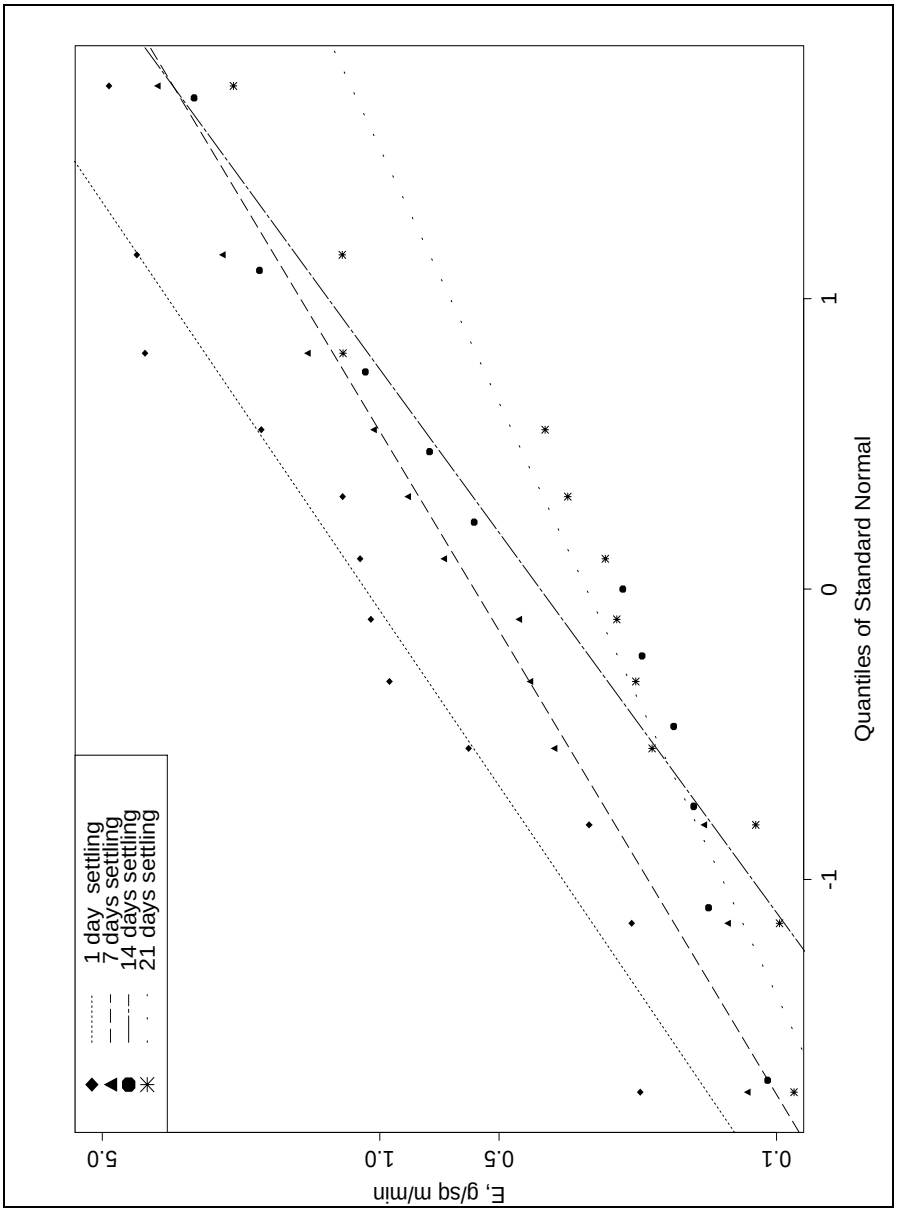

Figure 47. Cumulative probability distributions for various standing times plotted on standard deviation coordinates

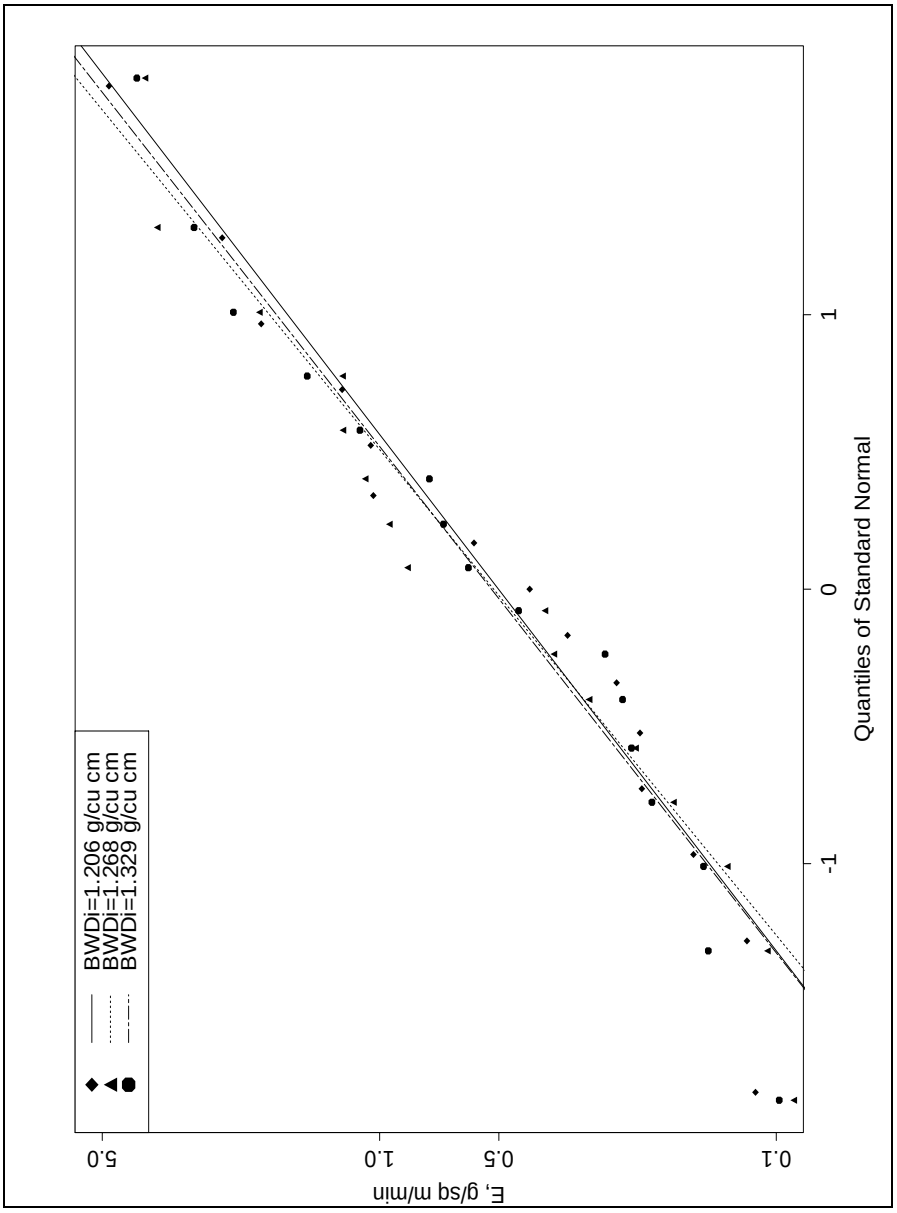

Figure 48. Cumulative probability distributions for various *BWD*'s plotted on standard deviation coordinates